

# Quantum Phase Transition of a Magnet in a Spin Bath

H. M. Rønnow,<sup>1,2,6\*</sup> R. Parthasarathy,<sup>2</sup> J. Jensen<sup>3</sup>,  
G. Aeppli<sup>4</sup>, T. F. Rosenbaum<sup>2</sup>, D. F. McMorrow<sup>4-6</sup>

<sup>1</sup>Laboratory for Neutron Scattering, ETH-Zürich and Paul Scherrer Institut,  
5232 Villigen, Switzerland

<sup>2</sup>The James Franck Institute and Department of Physics, The University of Chicago,  
IL 60637, USA

<sup>3</sup>Ørsted Laboratory, Niels Bohr Institute fAPG,  
Universitetsparken 5, 2100 Copenhagen, Denmark

<sup>4</sup>London Centre for Nanotechnology and Department of Physics and Astronomy,  
UCL, London, WC1E 6BT

<sup>5</sup>ISIS, RAL, UK

<sup>6</sup>Risø National Laboratory, DK-4000 Roskilde, Denmark

\*To whom correspondence should be addressed; E-mail: henrik.ronnow@psi.ch.

The excitation spectrum of a model magnetic system,  $\text{LiHoF}_4$ , has been studied using neutron spectroscopy as the system is tuned to its quantum critical point by an applied magnetic field. The electronic mode softening expected for a quantum phase transition is forestalled by hyperfine coupling to the nuclear spins. We show that interactions with the nuclear spin bath control the length scale over which the excitations can be entangled. This generic result limits how far it is possible to approach intrinsic electronic quantum criticality.

The preparation and preservation of entangled quantum states is particularly relevant for the development of quantum computers, where interacting qubits must produce states sufficiently long-lived for meaningful manipulation. The state lifetime, typically referred to as a decoherence time, is derived from coupling to the background environment. For solid state quantum

computing schemes, the qubits are typically electron spins, and they couple to two generic background environments (1). The oscillator-bath — *i.e.* delocalised environmental modes (2), such as thermal vibrations coupled via magneto-elastic terms to the spins — can be escaped by lowering the temperature to a point where the lattice is essentially frozen. Coupling to local degrees of freedom, such as nuclear magnetic moments which form a spin-bath, may prove more difficult to avoid, as all spin-based candidate materials for quantum computation have at least one naturally occurring isotope that carries nuclear spin. Experimental work on this subject has been largely restricted to the relaxation of single, weakly interacting, magnetic moments such as those on large molecules (3) while much less is known about spins as they might interact in a real quantum computer. In this regard, the insight that quantum phase transitions (4) are a good arena for looking at fundamental quantum properties of strongly interacting spins turns out to be valuable, as it has already been for explorations of entanglement. In particular, we show that coupling to a nuclear spin bath limits the distance over which quantum mechanical mixing affects the electron spin dynamics.

Quantum phase transitions (QPTs) are transitions between different ground states driven not by thermal fluctuations, but by quantum fluctuations controlled by some parameter such as doping, pressure and magnetic field (5, 6). Much of the interest in QPTs stems from their importance for understanding materials with unconventional properties – heavy Fermion systems and high temperature superconductors. However, these materials are rather complex, and do not easily lend themselves to a universal understanding of QPTs. To this end it is desirable to identify quantum critical systems with a well-defined and solvable Hamiltonian, and with a precisely controllable tuning parameter. One very simple model displaying a QPT is the Ising ferromagnet in a transverse magnetic field (7, 8, 9, 5), with the Hamiltonian:

$$\mathcal{H} = - \sum_{ij} J_{ij} \sigma_i^z \cdot \sigma_j^z - \Gamma \sum_i \sigma_i^x \quad (1)$$

In the absence of a magnetic field, the ensemble of the two degenerate  $\sigma^z = \pm 1$  states orders ferromagnetically below a critical temperature  $T_c$ . The transverse field  $\Gamma$  mixes the two states

and even at zero temperature leads to destruction of long-range order in a QPT at a critical field  $\Gamma_c$ . In the ferromagnetic state at zero field and temperature, the excitation spectrum is momentum independent and centered at the energy  $4 \sum_j \mathcal{J}_{ij}$  associated with single spin reversal. Upon application of a magnetic field, however, the excitations acquire a dispersion, softening to zero at the zone centre  $q = 0$  when the QPT is reached.

We investigate the excitation spectrum around the QPT in  $\text{LiHoF}_4$ , which is an excellent physical realisation of the transverse field Ising model, with an added term accounting for the hyperfine coupling between electronic and nuclear moments (11, 10, 12). The dilution series  $\text{LiHo}_x\text{Y}_{1-x}\text{F}_4$  is the host for a wide variety of collective quantum effects, ranging from tunnelling of single moments and domain walls to quantum annealing, entanglement and Rabi oscillations (13, 14, 15, 16, 17). These intriguing properties rely largely on the ability of a transverse field, whether applied externally or generated internally by the off-diagonal part of the magnetic dipolar interaction, to mix two degenerate crystal field states of each Ho ion. The Ho ions in  $\text{LiHoF}_4$  are placed on a tetragonal Scheelite lattice with parameters  $a = 5.175 \text{ \AA}$  and  $c = 10.75 \text{ \AA}$ . The crystal-field ground state is a  $\Gamma_{3,4}$  doublet with only a  $c$  component to the angular momentum and hence can be represented by the  $\sigma^z = \pm 1$  Ising states. A transverse field in the  $a$ - $b$  plane mixes the higher-lying states with the ground state producing a splitting of the doublet, equivalent to an effective Ising model field. The phase diagram of  $\text{LiHoF}_4$  (Fig. 1A) was determined earlier by susceptibility measurements (10), and displays a zero field  $T_c$  of 1.53 K, and a critical field of  $H_c = 49.5 \text{ kOe}$  in the zero temperature limit. The same measurements confirmed the strong Ising anisotropy, with longitudinal and transverse  $g$ -factors differing by a ratio of 18 (10). The sudden increase in  $H_c$  below 400 mK was explained by alignment of the Ho nuclear moments through the hyperfine coupling. Corrections to phase diagrams due to hyperfine couplings have a long history (18), and were noted for the  $\text{LiREF}_4$  ( $RE$ =Rare earth) series, of which  $\text{LiHoF}_4$  is a member, over twenty years ago (19). What is new here is that applying a transverse field and employing high resolution neutron scattering spectroscopy allows

us to carefully study the dynamics as we tune through the quantum critical point.

We measured the magnetic excitation spectrum of  $\text{LiHoF}_4$  using the TAS7 neutron spectrometer at Risø National Laboratory, with an energy resolution (full width at half maximum) of 0.06-0.18 meV (20). The transverse field was aligned to better than  $0.35^\circ$  and the sample cooled in a dilution refrigerator. At the base temperature of 0.31 K, giving a critical field of 42.4 kOe, the excitation spectrum was mapped out below, at and above the critical field (Fig. 2). For all fields a single excitation branch disperses upwards from a minimum gap at (2,0,0) towards (1,0,0). From (1,0,0) to (1,0,1), the mode shows little dispersion but appears to broaden. The discontinuity on approaching respectively  $(1, 0, 1 - \epsilon)$  and  $(1 + \epsilon, 0, 1)$  reflects the anisotropy and long-range nature of the magnetic dipole coupling. However, the most important observation is that the (2,0,0) energy, which is always lower than the calculated single ion energy ( $\sim 0.39$  meV at 42.4 kOe), shrinks on increasing the field from 36 to 42.4 kOe, and then hardens again at 60 kOe. At this qualitative level, what we see agrees with the mode softening predicted for the simple Ising model in a transverse field. However, it appears that the mode softening is incomplete. At the critical field of 42.4 kOe it retains a finite energy of  $0.24 \pm 0.01$  meV. Fig. 1B, showing the gap energy as a function of the external field, makes this result very apparent.

To obtain a quantitative understanding of our experiments we consider the full rare-earth Hamiltonian, which closely resembles that of  $\text{HoF}_3$  (21, 22). Each Ho-ion is subject to the crystal field, the Zeeman and the hyperfine coupling. The interaction between moments is dominated by the long-range dipole coupling, with a small nearest neighbour exchange interaction  $\mathcal{J}_{12}$ :

$$\begin{aligned} \mathcal{H} = & \sum_i \left[ \mathcal{H}_{\text{CF}}(\mathbf{J}_i) + A \mathbf{J}_i \cdot \mathbf{I}_i - g\mu_B \mathbf{J}_i \cdot \mathbf{H} \right] \\ & - \frac{1}{2} \sum_{ij} \sum_{\alpha\beta} \mathcal{J}_D D_{\alpha\beta}(ij) J_{i\alpha} J_{j\beta} - \frac{1}{2} \sum_{ij}^{n.n.} \mathcal{J}_{12} \mathbf{J}_i \cdot \mathbf{J}_j \end{aligned} \quad (2)$$

where  $\mathbf{J}$  and  $\mathbf{I}$  are respectively the electronic and nuclear moments, and for  $^{165}\text{Ho}^{3+}$   $J = 8$  and  $I = 7/2$ . Hyperfine resonance (23) and heat capacity measurements (24) show that the

hyperfine coupling parameter  $A = 3.36 \mu\text{eV}$  as for the isolated ion, with negligible nuclear-quadrupole coupling. The Zeeman term is reduced by the demagnetization field. The normalized dipole tensor  $D_{\alpha\beta}(ij)$  is directly calculable, and the dipole coupling strength is simply fixed by lattice constants and the magnetic moments of the ions at  $\mathcal{J}_D = (g\mu_B)^2 N = 1.1654 \mu\text{eV}$ . This leaves as free parameters various numbers appearing in the crystal field Hamiltonian  $\mathcal{H}_{\text{CF}}$  and the exchange constant  $\mathcal{J}_{12}$ . The former are determined (25) largely from electron spin resonance for dilute Ho atoms substituted for Y in  $\text{LiYF}_4$ , while the latter is constrained by the phase diagram determined earlier (10) (Fig.1 A). We have used an effective medium theory (9) previously applied to  $\text{HoF}_3$  (26) to fit the phase diagram, and conclude that a good overall description, except for a modest (14%) overestimate of the zero field transition temperature is obtained for  $\mathcal{J}_{12} = -0.1 \mu\text{eV}$ . Based on quantum Monte Carlo simulation data others (27) have also concluded that  $\mathcal{J}_{12}$  is substantially smaller than  $\mathcal{J}_D$ .

Having established a good parametrization of the Hamiltonian, we model the dynamics, where expansion to order  $1/z$  ( $z$  is the number of nearest neighbors of an ion in the lattice) leads to an energy dependent renormalization  $[1 + \Sigma(\omega)]^{-1}$  (of the order 10%) of the dynamic susceptibility calculated in the random phase approximation (RPA), with  $\Sigma(\omega)$  evaluated as described in (26). For the three fields investigated in detail, the dispersion measured by neutron scattering is closely reproduced throughout the Brillouin zone. As indicated by the solid lines in Fig. 2, the agreement becomes excellent if the calculated excitation energies are multiplied by a renormalization factor  $Z = 1.15$ . The point is not that the calculation is imperfect, but rather that it matches the data as closely as it does. Indeed, it also predicts a weak mode splitting of about  $0.08 \text{ meV}$  at  $(1, 0, 1 - \epsilon)$ , consistent with the increased width in the measurements. The agreement for the discontinuous jump between  $(1, 0, 1 - \epsilon)$  and  $(1 + \epsilon, 0, 1)$  due to the long-range nature of the dipole coupling, shows that this is indeed the dominant coupling.

Fig. 1B-C illustrates the simple origin of the incomplete softening and enhanced critical field, which is easiest to understand if we start from the polarised paramagnetic state above  $H_c$ ,

where the experiment, the purely electronic calculation, and the theory including the hyperfine coupling all coincide. At high fields the only effect of the hyperfine term is to split both the ground state and the electronic excitation modes into multiplets which are simply the direct products of the electronic and nuclear levels, with a total span of  $2A\langle J\rangle I \simeq 0.1$  meV as illustrated in Fig. 1C. Upon lowering the field, the electronic mode softens and would in the absence of hyperfine coupling reach zero energy at  $H_c^0 = 36$  kOe. The hyperfine coupling, however, mixes the original ground and excited (soft mode) states already above  $H_c$ . As this happens, the formation of a composite spin from mixed nuclear and electronic contributions immediately stabilizes ordering along the  $c$ -axis of the crystal. In other words, the hyperfine coupling shunts the electronic mode, raising the critical field to the observed  $H_c=42.4$  kOe, where the mode reaches a non-zero minimum. This process is accompanied by transfer of intensity from the magnetic excitation of electronic origin to much lower energy (in the  $10\ \mu\text{eV}$  range) soft modes of entangled nuclear/electronic character. Cooling to very low temperatures would reveal these modes as propagating and softening to zero at the quantum critical point, but at the temperatures reachable in our measurements there is thermalization, dephasing the composite modes to yield the strong quasi-elastic scattering appearing around  $Q = (2, 0, 0)$  and zero energy at the critical field, as in Fig. 2.

The intensities of the excitations are simply proportional to the matrix elements  $|\langle f | \sum_j \exp(iQ \cdot R_j) J_j^+ | 0 \rangle|^2$ , and therefore provide a direct measure of the wavefunctions via the interference effects implicit in the spatial Fourier transform of  $J_j$ . Fig. 3 shows intensities recorded along  $(h, 0, 0)$  for the three fields 36, 42.4, and 60 kOe. They follow a momentum dependence characterized by a broad peak near  $(2,0,0)$ , which is well described by our theory. In the absence of hyperfine interactions, the intensity at  $H_c^0$  would diverge as  $q$  approaches  $(2, 0, 0)$ , reflecting that the real-space dynamical coherence length  $\xi_c$  of the excited state grows to infinity. The finite width of the peak observed at  $H_c$ , corresponds in real space to a distance of order the inter-holmium spacing, and implies that because they forestall the softening of the electronic mode,

the hyperfine interactions also limit the distance over which the electronic wavefunctions can be entangled (4). Thus, Fig. 3 is a direct demonstration of the limitation of quantum coherence in space via coupling to a nuclear spin bath. The dynamical length  $\xi_c$  is obtained from a sum over matrix elements connecting the ground state to a particular set of excited states, while the thermodynamic correlation length  $\xi_t$  is derived from the equal time correlation function  $S(r)$  which is the sum over all final states.  $\xi_t$  diverges at second order transitions such as those in  $\text{LiHoF}_4$ , where the quasielastic component seen in our data dominates the long-distance behaviour of  $S(r)$  at  $T_c(H)$ . It is the electronic mode and hence  $\xi_c$  that dictates to which extent  $\text{LiHoF}_4$  can be characterised and potentially exploited as a realisation of the ideal transverse field Ising model.

Beyond providing a quantitative understanding of the excitations near the quantum critical point of a model experimental system, we obtain new insight by bringing together the older knowledge from rare-earth magnetism and the contemporary ideas of entanglement, qubits and decoherence. While the notion of the spin-bath was developed to address decoherence in localised magnetic clusters and molecules (1), our work discloses its significance for quantum phase transitions. Notably, we establish that the spin bath is a generic feature that will limit how far it is possible to observe intrinsic electronic quantum criticality. While this may not be a significant factor when thinking about transition metal oxides with very large exchange constants, it could matter for rare earth and actinide intermetallic compounds which show currently unexplained cross-overs to novel behaviours at low ( $< 1$  K) temperatures (see e.g. (28)).

For magnetic clusters, decoherence can be minimised in a window between the oscillator-bath dominated high temperature and the spin-bath dominated low-temperature regions (29). Our calculations suggest that the dense quantum critical magnet shows analogous behaviour. Here the interacting electron spins themselves constitute the oscillator bath, and the extent to which the magnetic excitation softens at  $T_c(H)$ , measured by the ratio of the zone center energy  $E_c$  to the field-induced single ion splitting  $\Delta$  (Fig. 1D), gauges the electronic decoherence.

$E_c/\Delta$  achieves its minimum not at  $T = 0$ , but rather at an intermediate temperature  $T \simeq 1$  K, exactly where the phase boundary in Fig. 1A begins to be affected by the nuclear hyperfine interactions.

## References

1. N. V. Prokof'ev, P. C. E. Stamp, *Rep. Prog. Phys* **63**, 669 (2000).
2. R. P. Feynman, F. L. Vernon, *Ann. Phys* **24**, 118 (1963).
3. W. Wernsdorfer, S. Bhaduri, R. Tiron, D. N. Hendrickson, G. Christou, *Phys. Rev. Lett.* **89**, 197201 (2002).
4. A. Osterloh, L. Amico, G. Falci, R. Fazio, *Nature* **416**, 608 (2002).
5. S. Sachdev, *Physics World* **12**, 33 (1999).
6. S. Sachdev, *Quantum Phase Transitions* (Cambridge University Press, Cambridge, 1999).
7. P. G. de Gennes, *Solid State Commun.* **1**, 132 (1963).
8. R. J. Elliott, P. Pfeuty, C. Wood, *Phys. Rev. Lett.* **25**, 443 (1970).
9. R. B. Stinchcombe, *J. Phys. C* **6**, 2459 and 2484 (1973).
10. D. Bitko, T. F. Rosenbaum, G. Aeppli, *Phys. Rev. Lett.* **77**, 940 (1997).
11. T. F. Rosenbaum, *et al.*, *J. Appl. Phys.* **70**, 5946 (1991).
12. D. Bitko, Order and disorder in a model quantum magnet, Thesis, University of Chicago, Illinois (1997).
13. R. Giraud, *et al.*, *Phys. Rev. Lett.* **87**, 057203 (2001).
14. J. Brooke, *et al.*, *Science* **284**, 779 (1999).



15. J. Brooke, T. F. Rosenbaum, G. Aeppli, *Nature* **413**, 610 (2001).
16. S. Ghosh, *et al.*, *Science* **296**, 2195 (2002).
17. S. Ghosh, *et al.*, *Nature* **425**, 48 (2003).
18. K. Andres, *Phys. Rev. B* **7**, 4295 (1973).
19. R. W. Youngblood, G. Aeppli, J. d. Axe, J. A. Griffin, *Phys. Rev. Lett.* **49**, 1724 (1982).
20. For details, request H. M. Rønnow, Aspects of quantum magnetism in one, two and three dimensions, Thesis, Risø National Laboratory, Denmark (2000).
21. M. J. M. Leask, *et al.*, *J. Phys. C* **6**, 505 (1994).
22. A. P. Ramirez, J. Jensen, *J. Phys. C* **6**, L215 (1994).
23. J. Magariño, P. J. Tuchendler, Beauvillain, I. Laursen, *Phys. Rev. B* **21**, 18 (1980).
24. G. Mennenga, L. J. de Jongh, W. J. Huiskamp, *J. Magn. Magn. Mater* **44**, 59 (1984).
25. H. M. Rønnow *et al.*, *In preparation*.
26. J. Jensen, *Phys. Rev. B* **49**, 11833 (1994).
27. P. B. Chakraborty, P. Henelius, H. Kjønsberg, A. W. Sandvik, S. M. Girvin, *Phys. Rev. B* **70**, 144411 (2004).
28. P. Gegenwart, *et al.*, *Phys. Rev. Lett.* **89**, 056402 (2002).
29. P. C. E. Stamp, I. S. Tupitsyn, *Phys. Rev. B* **69**, 014401 (2004).
30. We thank G. McIntyre for his expert assistance during complementary measurements on the D10 diffractometer at the Institut Laue Langevin, Grenoble, France. Work at the University of Chicago was supported primarily by the NSF MRSEC Program under DMR-0213745.

Work in London was supported by the Wolfson-Royal Society Research Merit Award Program and the Basic Technologies program of the UK Research Councils.

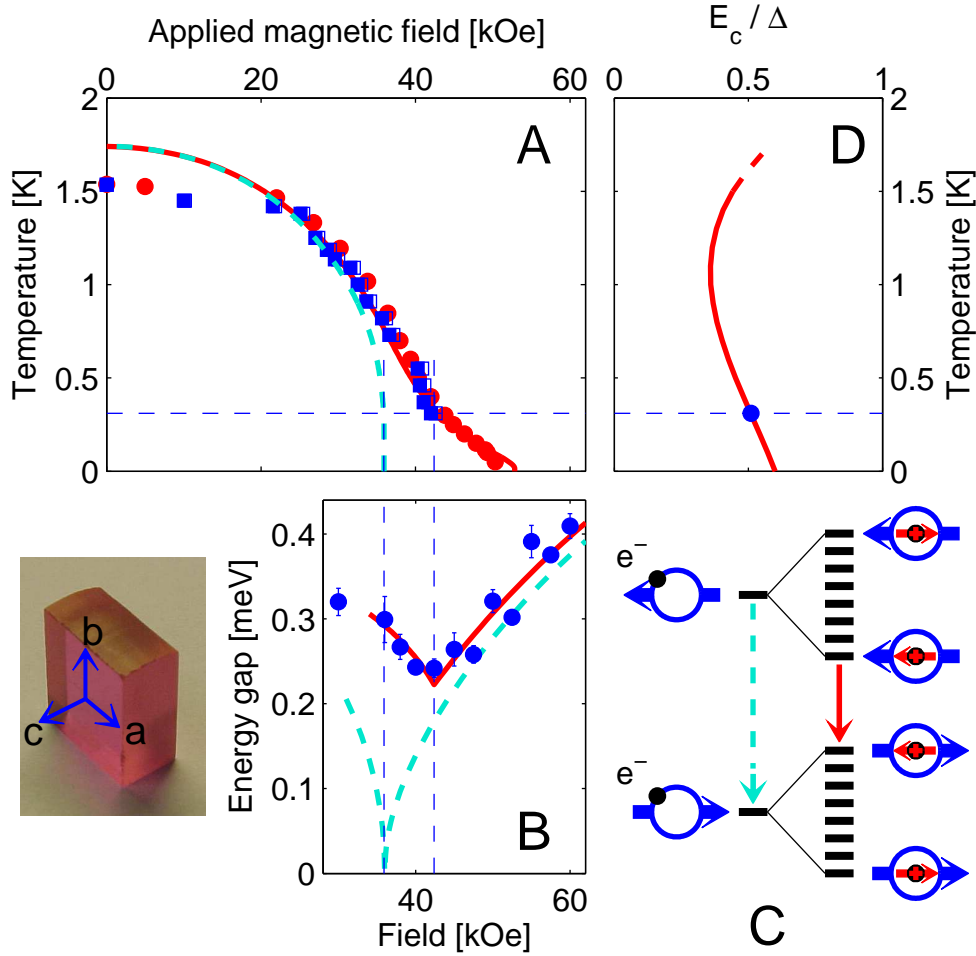


Figure 1: **A** Phase diagram of LiHoF<sub>4</sub> as a function of transverse magnetic field and temperature from susceptibility ( $\chi$ ) (circles) and neutron scattering (squares) measurements. Lines are  $1/z$  calculations with (solid) and without (dashed) hyperfine interaction. Horizontal dashed guide marks the temperature 0.31 K at which inelastic neutron measurements were performed. **B** Field dependence of the lowest excitation energy in LiHoF<sub>4</sub> measured at  $Q = (1 + \epsilon, 0, 1)$ . Lines are calculated energies scaled by  $Z = 1.15$  respectively with (solid) and without (dashed) hyperfine coupling. The dashed vertical guides show how in either case the minimum energy occurs at the field of the transition (c.f. **A**). **C** Schematic of electronic (blue) and nuclear (red) levels as the transverse field is lowered towards the QCP. Neglecting the nuclear spins, the electronic transition (light blue arrow) would soften all the way to zero energy. Hyperfine coupling creates a non-degenerate multiplet around each electronic state. The QCP now occurs when the excited state multiplet through level repulsion squeezes the collective mode of the ground state multiplet to zero energy, hence forestalling complete softening of the electronic mode. Of course, the true ground and excited states are collective modes of many Ho ions and should be classified in momentum space. **D** Calculated ratio  $E_c/\Delta$  of the minimum excitation energy  $E_c$  to the single ion splitting  $\Delta$  at the critical field as a function of temperature. This measures how far the electronic system is from the coherent limit, for which  $E_c/\Delta = 0$ .

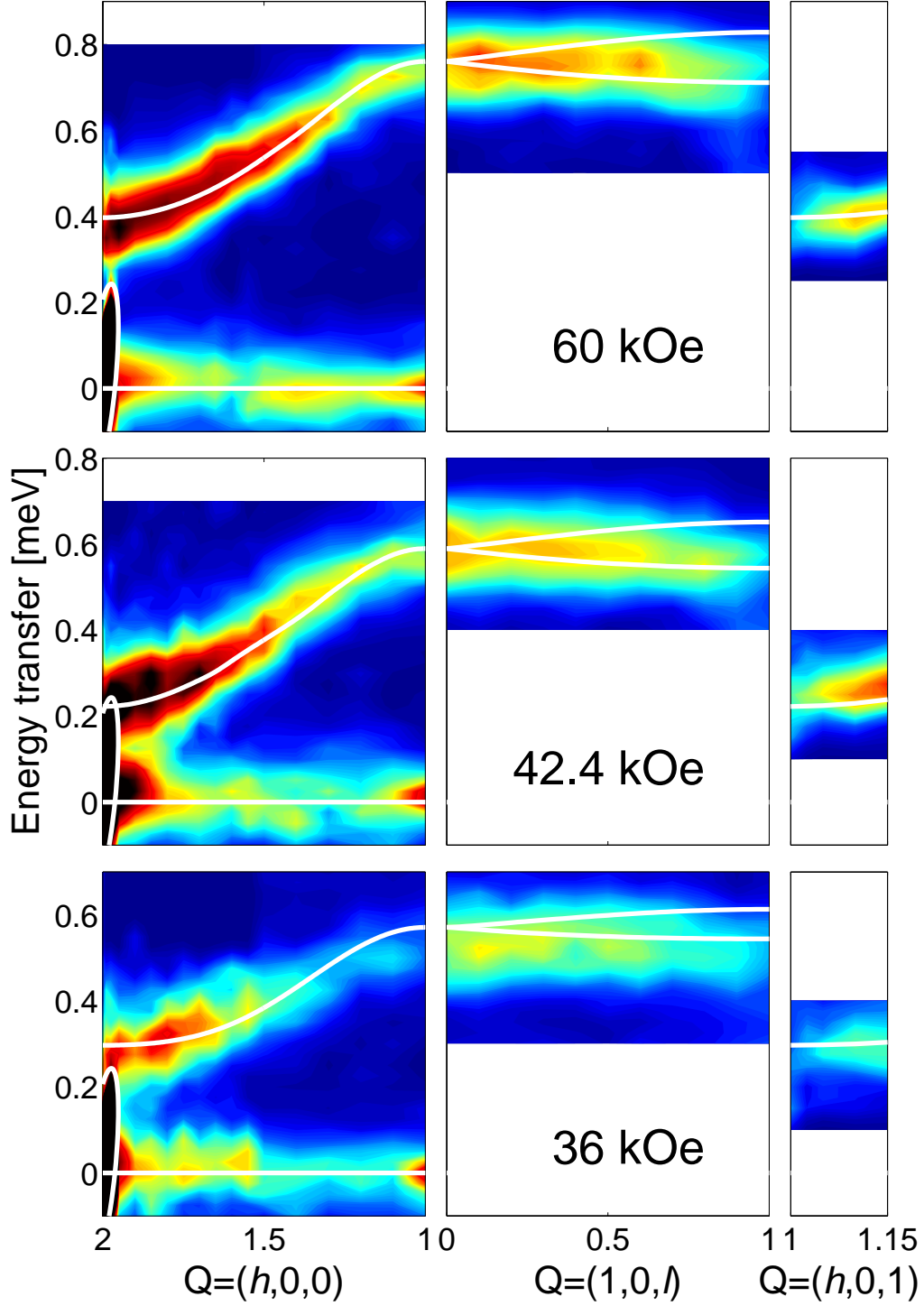


Figure 2: Pseudocolor representation of the inelastic neutron scattering intensity for  $\text{LiHoF}_4$  at  $T = 0.31$  K observed along the reciprocal space trace  $(2, 0, 0) \rightarrow (1, 0, 0) \rightarrow (1, 0, 1) \rightarrow (1.15, 0, 1)$ . White lines show the  $1/z$  calculation for the excitation energies as described in the text. White ellipses around the  $(2, 0, 0)$  Bragg peak indicate 5 times the full-width-half-max resolution tail.

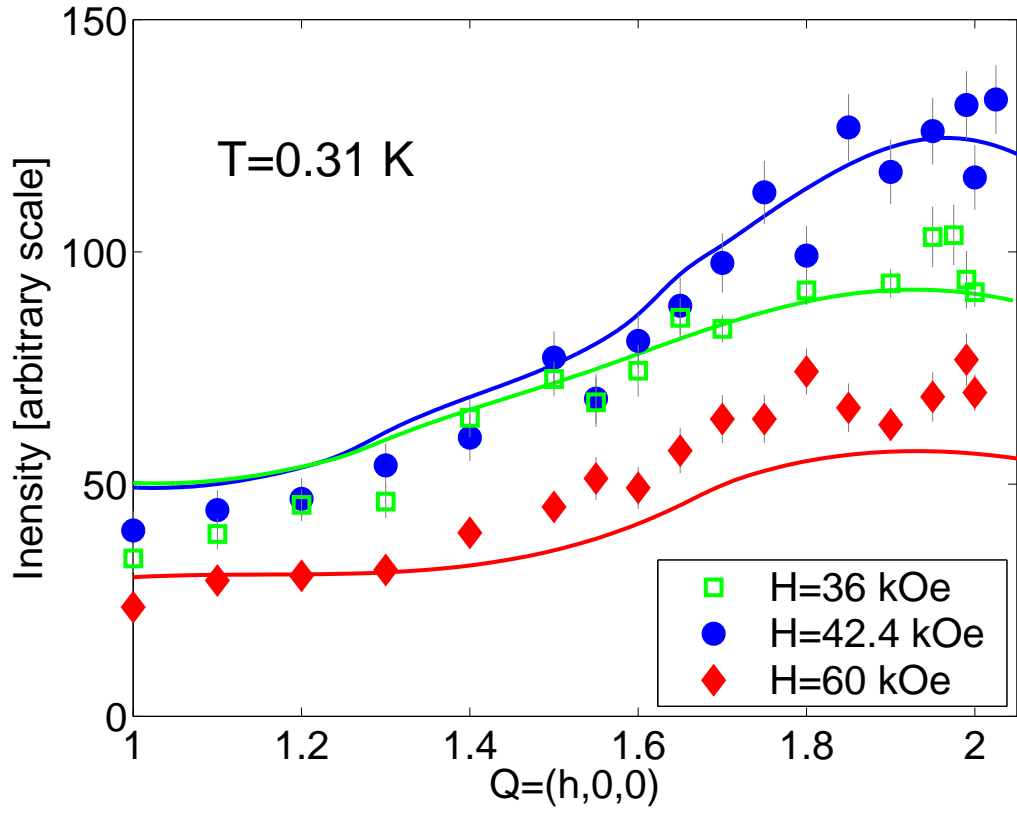


Figure 3: Measured intensities of the excitations along  $Q = (h, 0, 0)$  at the same values of the field as in Fig. 2. Lines are calculated with geometric and resolution corrections applied to allow comparison to the neutron data.